

## Coupled impact of decadal precipitation and evapotranspiration on peatland degradation in the Zoige basin, China

Zhiwei Li, Peng Gao, Xuyue Hu, Yujun Yi, Baozhu Pan & Yuchi You

To cite this article: Zhiwei Li, Peng Gao, Xuyue Hu, Yujun Yi, Baozhu Pan & Yuchi You (2019): Coupled impact of decadal precipitation and evapotranspiration on peatland degradation in the Zoige basin, China, Physical Geography, DOI: [10.1080/02723646.2019.1620579](https://doi.org/10.1080/02723646.2019.1620579)

To link to this article: <https://doi.org/10.1080/02723646.2019.1620579>



Published online: 27 May 2019.



Submit your article to this journal [↗](#)



Article views: 21



View Crossmark data [↗](#)

ARTICLE



# Coupled impact of decadal precipitation and evapotranspiration on peatland degradation in the Zoige basin, China

Zhiwei Li <sup>a,b</sup>, Peng Gao<sup>c</sup>, Xuyue Hu<sup>b</sup>, Yujun Yi<sup>d</sup>, Baozhu Pan<sup>e</sup> and Yuchi You<sup>b</sup>

<sup>a</sup>State Key Laboratory of Plateau Ecology and Agriculture, Qinghai University, Xining, China; <sup>b</sup>School of Hydraulic Engineering, Key Laboratory of Water-Sediment Sciences and Water Disaster Prevention of Hunan Province, Changsha University of Science & Technology, Changsha, China; <sup>c</sup>Department of Geography, Syracuse University, New York, USA; <sup>d</sup>State Key Laboratory of Water Environment Simulation and Pollution Control, School of Environment, Beijing Normal University, Beijing, China; <sup>e</sup>State Key Laboratory Base of Eco-hydraulic Engineering in Arid Area, Xi'an University of Technology, Xi'an, China

## ABSTRACT

This study quantified the temporal properties of precipitation and actual evapotranspiration (ETa) in the Zoige basin of the Yellow River source region, China during the 1967–2011 period, as well as their influence to the area reduction of peatland. We extracted areas of different land-use and land-cover (LULC) types and obtained daily precipitation data. Then, we calculated annual precipitation (AP) and specific cumulative precipitation (SCP), which is the sum of precipitation to the date when an image was taken, and showed that the peatland areas were strongly affected by SCP. Using a modified Penman–Monteith equation, we calculated ETa for each LULC type and the area-weighted ones to show that the area-weighted total ETa was mainly contributed from grassland and peatland, which was between 450 and 550 mm. Temporal trends of the ratio of SCP to evapotranspiration showed that precipitation was generally greater than evapotranspiration rate not only during the summer but also over the 1967–2011 period. This trend failed to completely explain the continuous decrease of peatland area in the Zoige basin in decades. The draining effect of artificial ditches and natural gullies might play an additional role in causing peatland degradation but requires further process-based studies.

## ARTICLE HISTORY

Received 30 November 2018  
Accepted 15 May 2019

## KEYWORDS

Peatland degradation;  
specific cumulative  
precipitation;  
evapotranspiration; Zoige  
basin

## Introduction

Wetlands occupy 5–8% of the total solid area on the Earth surface (Mitsch & Gosselink, 2015). They form a complex and integrated terrestrial and aquatic ecosystem, and serve as a crucial center of global carbon sequestration by storing 20–30% of the global organic carbon (Mitra, Wassmann, & Vlek, 2005; Mitsch et al., 2013; Mitsch & Gosselink, 2015; Xiang, Guo, Wu, & Sun, 2009). Because of their irreplaceable functions (e.g. colation, filtration, and sedimentation), wetlands have been widely studied for their biodiversity, hydrological cycle, and carbon cycle. As an important part of wetlands, nevertheless, worldwide peatlands have suffered from area reduction and function degeneration due to

**CONTACT** Peng Gao  [pegao@maxwell.syr.edu](mailto:pegao@maxwell.syr.edu)

This article has been republished with minor changes. These changes do not impact the academic content of the article.

© 2019 Informa UK Limited, trading as Taylor & Francis Group

global warming and human activities in recent decades (Li, Gao, & You, 2018; Mitsch et al., 2013; Niu et al., 2012; Sica, Quintana, Radeloff, & Gavier-Pizarro, 2016; Song et al., 2014). These problems are particularly true in the fragile peatlands of Zoige basin, located on the eastern side of the Qinghai–Tibet Plateau (Jiang, Lv., Chen, & Liu, 2017; Li et al., 2015; Yang et al., 2017; Yu, Lehmkuhl, & Falk, 2017; Zhang et al., 2014). It has been well known that meteorological factors (e.g. precipitation and evapotranspiration) have played key roles in maintaining natural processes of peatlands (Cui et al., 2015; B. Li et al., 2014, 2013; Sprenger, Tetazlaff, Tunaley, Dick, & Soulsby, 2017; Sun et al., 2011; Yao, Han, & Xu, 2010). Therefore, rehabilitating deteriorated peatlands in the Zoige basin requires understanding how these climatic factors change over time.

Zoige basin is an area with elevations ranging between 3400 and 3900 m. It has the world's largest alpine peatland that bears a very high value of ecosystem services (Li, Wang, & Pan, 2016; Wang et al., 2015; Yang et al., 2017; Zhang & Lu, 2010). Their existence is critical for water resource utilization, ecological protection, and regional social-economic development in the Upper Yellow River region (Bian, Li, & Deng, 2010; Li et al., 2016; Tan et al., 2011; Xiang et al., 2009; Yang et al., 2017). However, the peatland area has decreased by approximately 25% from 4600 to 3450 km<sup>2</sup> since the 1950s (Li, Zhao, Gao, Sun, & Li, 2011; Xiang et al., 2009; Zhang et al., 2014; Zhang, Wang, & Wang, 2011), which could be partially related to temporal changes of local climate. Dominated by alpine climate and summer monsoon weather, the Zoige peatland is characterized by its significant seasonal variation, with the saturated area primarily controlled by concentrated precipitation in the wet season from May to September. Although the influence of the intra-annual variation of precipitation on wetland distribution, vegetation cover, and local desertification has been noticed (Hu, Dong, Lu, & Yan, 2015; Yu et al., 2017), it has not been a focus in these studies.

Examining the impact of precipitation on peatland requires calculating temporal changes of peatland areas. The most commonly used method is extracting areas of different land use and land covers (LULCs) and their temporal changes from some historical series of multi-source satellite images (Landsat TM/OLI after 1980) based on different colors and/or spectral signals from surfaces of different LULC types (Gong et al., 2010; Jiang et al., 2017; Li et al., 2011; Zhang, Yi, Song, Kimball, & Lu, 2016). Unfortunately, area extraction in previous studies suffered three types of inconsistency. First, some studies used visual interpretation of spectral signals in the images based on either unsupervised or supervised classification (Bai, Hua, Cui, Wang, & Chen, 2008; Fan, 1988; Hu, Dong, Lu, & Yan, 2012; Li et al., 2011), while some directly measured the area from a high-resolution (1:10,000) topographic map with the help of the 5-year field survey data and remote sensing images (Sun, 1992). Still some studies did not elaborate the extraction method at all (Gao, 2006; Li, Erickson, Peresta, & Drake, 2010; Zhang et al., 2011). Second, the measured peatland areas may be wetland, swamp, or peatland (Bai et al., 2008; Gao, 2006; Hu et al., 2012; Li et al., 2011; Zhang et al., 2011). However, the areas of a swamp and peatland in the same imagery could be significantly different. Third, many studies used administrative boundaries of local counties (e.g. Aba, Zoige, Hongyuan, Maqu) to define the Zoige basin (Bai et al., 2008; Hu et al., 2012; Li et al., 2010, 2011; Zhang et al., 2011), but these defined areas are much larger than that of the Zoige watershed. Therefore, the peatland areas determined from these studies are not comparable. It is thus essential to use a clearly defined extraction method to calculate peatland area based on the watershed that covers the Zoige basin.

Evapotranspiration is a key indicator of the effect of climate warming on natural environment (Glenn et al., 2013; Li et al., 2010; Raddatz, Papakyriakou, Swystun, & Tenuta, 2009; Sprenger et al., 2017; Zhou & Zhou, 2009). Specifically, global warming increases air temperature and evapotranspiration of land surface (Bai, Lu, Wang, et al., 2013; Li et al., 2014; Niu et al., 2012; Zhang et al., 2016). Based on this assertion, the increase of evapotranspiration has been linked to surface water loss and peatland degradation (Hu, Maskey, & Uhlenbrook, 2011; Li et al., 2014; Zhang et al., 2016). Therefore, full understanding of the causes of the peatland reduction in the Zoige basin also needs to consider the temporal changes of evapotranspiration.

However, the complexity of soil-vegetation-atmosphere system makes estimating the actual evapotranspiration more difficult than other elements in a hydrological cycle (Carlson Mazur, Wiley, & Wilcox, 2014; Li et al., 2013; Wang et al., 2013). Thus far, there exist dozens of formulae for estimating evapotranspiration that are based on lysimeter measurements, energy balance, aerodynamics, isotope analysis, eddy correlation analysis, remote sensing analysis, and synthesis inversion. Each of these methods focuses on different physical aspects of evapotranspiration and hence has different applications. For the grassland and peatland in China, the lysimeter, Penman–Monteith (P-M), and Takahashi Koichi (T-K) methods have been widely used, though the remote sensing method was also used to estimate evapotranspiration of a large area (e.g. Qinghai–Tibet Plateau) (Zhao, Jing, Chen, & Kun, 2009). As for the Zoige basin, the first three (i.e. lysimeter, P-M, and T-K) methods have been used, but the results of these calculations were inconsistent. Studies using the lysimeter method led to estimates annual evapotranspiration in the Zoige basin as high as 1000 mm (Liu et al., 2016; Wang, Wang, & Wang, 2015). Use of the P-M and the T-K methods produced the estimated annual evapotranspiration about 700–820 mm (Wang et al., 2015) and 240–300 mm (Guo & Li, 2007), respectively. Although differences among these formulas may contribute to the discrepancies of the calculated annual evapotranspiration, the main cause of these discrepancies might be ascribed to limitations in the use of these formulas. In other words, these formulas ignored the fact that different LULC types in the Zoige basin may generate different values of evapotranspiration under the same meteorological conditions. Therefore, determining the actual evapotranspiration must account for spatially variable LULC types.

The goal of this study was to assess whether or not climate change is the main driver of peatland degradation in the Zoige basin. The study had three specific objectives: (1) estimating rainfall-induced errors in calculation of the peatland area by examining the relationship between apparent peatland area and cumulative precipitation; (2) accurately determining evapotranspiration by accounting for variable contributions from different LULC types in the Zoige basin; and (3) understanding temporal changes of the cumulative precipitation and evapotranspiration in the 1967–2011 period.

## Materials and methodology

### *Study area and data sources*

Zoige basin is located in the Yellow River source region, the northeast side of the Qinghai–Tibet Plateau (Figure 1(a, b)). It has elevations ranging between 3400 and 3900 m above sea level and thus is a typical alpine region. The Zoige basin has an area

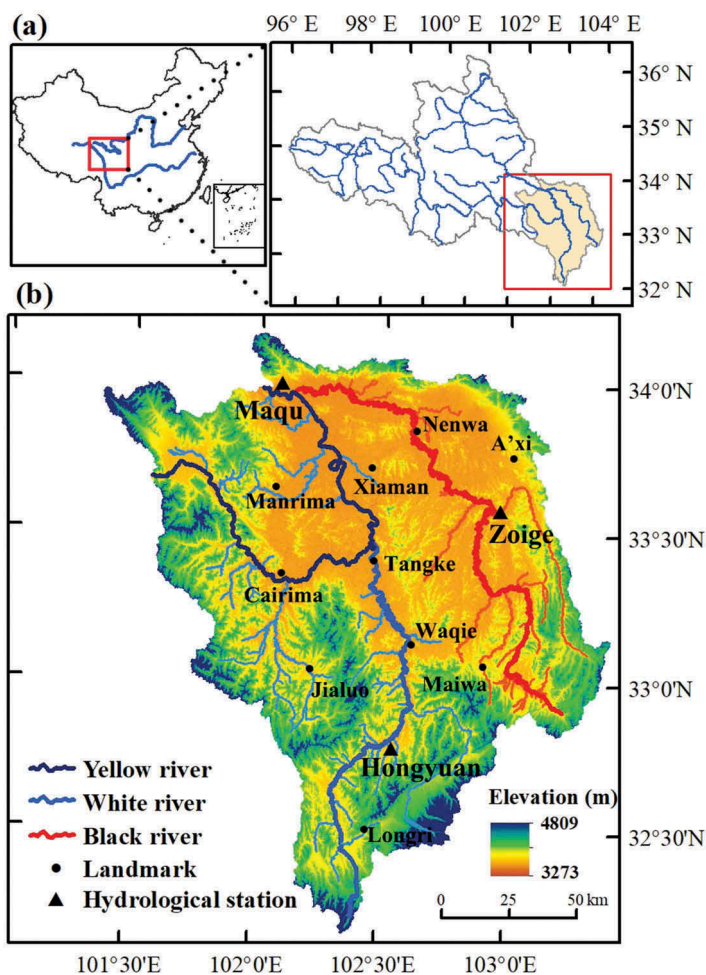


**Figure 1.** Location of the Zoige basin in the Upper Yellow River Region and basin topography. (a) Detailed location of the Zoige basin within the Upper Yellow River watershed, China; (b) Topographic structure of the Zoige basin. The black triangles represent three local weather stations whose data were used in this study: Zoige, Hongyuan, and Maqu. Blue lines represent the mainstream network within the basin.

of  $\sim 22,000 \text{ km}^2$ , which administratively belongs to Hongyuan, Zoige, Aba, and Maqu Counties. It has a continental alpine and monsoon climate, warm and humid between May and September (i.e. the wet season), and cold and dry between October and April (i.e. the dry season). Its ranges of annual average temperature, relative humidity, and potential evapotranspiration are  $0.6\text{--}1.2^\circ\text{C}$ ,  $64\text{--}73\%$ , and  $1100\text{--}1274 \text{ mm}$ , respectively. The mean annual precipitation of the Zoige basin is between  $560$  and  $860 \text{ mm}$ , about  $60\%$  to  $80\%$  of which is concentrated in summer when rainfall is frequent. Vegetation in peatlands is mainly alpine meadow that has the dominant species of *Carex muliensis*, *Carex meyeriana*, *Kobresia tibetica*, and *Blysmus sinocompressus*, *Deschampsia cespitosa*, *Pedicularis sp.* mainly in grassland (Sun, 1992). As an important water source of the Upper Yellow River (UYR), the Zoige basin supplies  $\sim 4\text{--}5$  billion  $\text{m}^3$  of water annually to

the UYR, which takes about 20% of the measured annual runoff in the UYR at the Maqu hydrological station (Li, Hao, Wang, Wang, & Yu, 2008; Li et al., 2015). This nature is largely ascribed to the fact that the basin contains widely distributed peatlands, which were formed about 10,000 years ago under a cold and wet climate (Wang et al., 2015; Zhao et al., 2014; Zhao, Yu, & Zhao, 2011).

Both meteorological and remote sensing data were obtained from different sources and subsequently analyzed in this study. Meteorological data were obtained from Zoige (33.35° N, 102.58° E), Hongyuan (32.48° N, 102.33° E), and Maqu (34.00°N, 102.05°E) stations whose altitudes are 3439.6, 3491.6, and 3471.4 m, respectively (Figure 1(c)). These stations are maintained by the National Meteorological Information Center of China. The obtained data include daily rainfall amount, temperature, sunshine duration, wind speed, air pressure, and relative humidity in the Zoige (1957–2011), Hongyuan (1961–2011), and Maqu stations (1967–2011). These data were used to calculate different types of precipitation and actual evapotranspiration. The remote sensing images, downloaded from the spatial data cloud of China (<http://www.gscloud.cn>), included Landsat TM and OLI\_TIRS data with 30-m resolution. Because the study area is covered by several standard scenes, the image for the study area was created by mosaicking these scenes obtained on the same date. The requirement of multiple scenes for the study area limited the number of usable images, and the final Landsat imagery covering the Zoige basin ranged from 1990 to 2016.

### **Precipitation calculation**

Given that the time series of available daily precipitation in the three (Zoige, Hongyuan, and Maqu) stations (Figure 1(c)) had different starting years, data compiled from these stations were trimmed to their common period, from 1967 to 2011. Annual precipitation (AP) was calculated by summing all daily precipitation in that year. Annual specific cumulative precipitation (SCP) was calculated such that its starting date was always 1 January and ending date was consistent with that of an available Landsat image in the same year. For instance, if an available Landsat image was taken on 17 September 2000, then the SCP for that year was calculated by summing the daily precipitation from 1 January up to the same date. In addition to AP and SCP, the spatially distributed daily precipitation across the entire study area was generated using the kriging interpolation method in ArcGIS 10.2. This data were subsequently used to estimate the SCP for the specific area that was included in a complete time series of Landsat images from May to October in 2008 (the only available monthly images) for illustrating the correlation of temporal changes between SCP and LULC types in 2008.

### **Area extraction for different LULC types**

Areas of different LULC types including grassland, peatland, forestland, water body, desertified land, and construction land were extracted from a series of satellite images from 1990 to 2016 using the rule based on feature extraction workflow in ENVI 5.3. The general extraction procedure (Figure 2) may be summarized as follows:

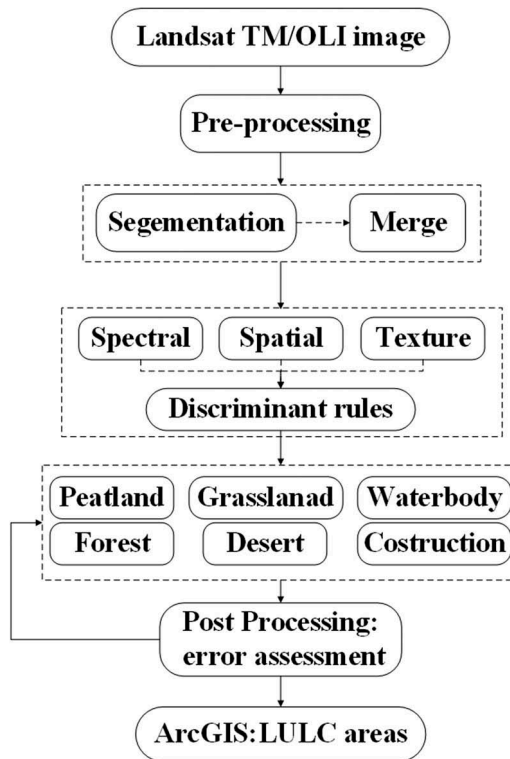


**Figure 2.** Flow chart showing the procedure of extracting areas of different LULC types from a satellite image.

Each original image (Landsat TM or OLI) was pre-processed in ENVI 5.3 to make it ready for analysis. Next, the image was spatially segmented into small elements. These elements were subsequently merged to form groups of different sizes, each of which had similar brightness, spectral, and texture characteristics (Figure 2). These groups were determined by adjusting two parameters of the edge-separation algorithm (Clinton, Holt, Scarborough, Yan, & Gong, 2010; Neubert & Herold, 2008) in ENVI 5.3 with the aid of visual interpretation. After this step, discriminant rules for identifying extents of different LULC types were established based on three aspects of the groups: spectral ranges, spatial patterns, and texture characteristics (Figure 2). The extents of each LULC type were then identified from the image and processed (mainly including orthorectification, FLASSH atmospheric correction, and boundary correction) using models available in ENVI 5.3. Post-processing was featured by error assessment, which led to the kappa coefficient of 0.839 and the total accuracy of 86.67%. These errors were further assessed by comparing a set of sample random points (165) from all LULC types of an image with the same set of points independently obtained from the Google Earth images of the same year (0.6 m resolution). About 87% of the points were correctly identified using this method. These error estimations suggested that the identified LULC types were accurate. Finally, the area of each LULC type was calculated in ArcGIS 10.2 (Figure 2).

The obtained series of the areas for each LULC type from 1990 to 2016 was used, together with the calculated annual and cumulative precipitation, to develop empirical relationships among these parameters. It should be noted that rather than judging by physical properties of peat underground, the peatland area determined using this method includes those of dry peat whose surface vegetation is different from that of grassland and saturated water pond (i.e. swamp) that may cover either peatland or grassland. Because the size of swamp is sensitive to precipitation, it may vary even within one year, causing uncertainties in area extraction. This problem was demonstrated and solved by relating the peatland area identified in four different months of 2008 when the satellite images were available to the associated SCP.

### Evapotranspiration calculation

Among many existing formulas, the Penman–Monteith (P-M) formula, which combines the principle of energy balance and water vapor diffusion theory, is most widely used for calculating evapotranspiration (Allen, Pereira, Raes, & Smith, 1998). By focusing on the physiological characteristics of crops, the P-M formula was modified by Food and Agriculture Organization (FAO) of the United Nations (Allen et al., 1998), which led to the FAO56 P-M method that has been used for determining evapotranspiration in wetlands around the world (Abteu, Obeysekera, & Iricanin, 2011; Jacobs, Mergelsberg, Lopera, & Myers, 2002; Lott & Hunt, 2001; Mao, Bergman, & Tai, 2002; Wossenu, 1996). Different from the earlier calculations of the potential evapotranspiration in the Zoige basin, our equation specifically considered the different impacts of the four LULC types (i.e. grassland, peatland, water body, and desertified land) on the actual evapotranspiration ( $ET_{a,t}$ ) in the Zoige basin:

$$ET_{a,t} = \frac{A_g \cdot ET_{a,g} + A_p \cdot ET_{a,p} + A_w \cdot ET_{a,w} + A_d \cdot ET_{a,d}}{A_g + A_p + A_w + A_d} \quad (1)$$

where  $ET_{a,g}$ ,  $ET_{a,p}$ ,  $ET_{a,w}$ , and  $ET_{a,d}$  are the actual evapotranspiration/evaporation of grassland, peatland, water body, and desertified land, respectively,  $A_g$ ,  $A_p$ ,  $A_w$ , and  $A_d$  are the area of grassland, peatland, water body, and desertified land, respectively. In this LULC classification, forestland was lumped into grassland rather than treated as a separate type, as the P-M formula was not designed for forestland. Since the area of the forestland was only 0.26% of the total area, this treatment should not affect the calculated values of  $ET_{a,t}$ . Similarly, because construction land only occupied 0.12% of the total area, we assumed that its contribution to  $ET_{a,t}$  is negligible.

Determination of the actual evapotranspiration requires calculating evapotranspiration for a “reference crop” ( $ET_0$ ), defined in the FAO56’s *Drainage and Irrigation Handbook* as “A hypothetical crop, assuming a height of 0.12 m, with a fixed surface resistance of  $70 \text{ s m}^{-1}$  and a reflectivity of 0.23” (Allen et al., 1998). This definition has led to an internationally accepted method, the FAO56 P-M formula for determining  $ET_0$ :

$$ET_0 = \frac{0.408\Delta(R_n - G) + \gamma \frac{900}{T+273} u_2 (e_s - e_a)}{\Delta + \gamma(1 + 0.34u_2)} \quad (2)$$

where  $R_n$  is the net radiation on the surface of the crop ( $\text{MJ}/\text{m}^2 \cdot \text{day}$ ),  $G_s$  is the soil heat flux ( $\text{MJ}/\text{m}^2 \cdot \text{day}$ ),  $T$  is the daily average temperature at the height 2 m above the ground ( $^\circ\text{C}$ ) and calculated by  $T = \frac{T_{\max} + T_{\min}}{2}$ ,  $T_{\max}$  and  $T_{\min}$  ( $^\circ\text{C}$ ) are the daily maximum and minimum air temperature, respectively,  $u_2$  is the wind speed at the same height (m/s),  $e_s$  is the saturated vapor pressure (kPa),  $e_a$  is the actual vapor pressure (kPa),  $\Delta$  is the curve slope of saturated water vapor pressure, and  $\gamma$  is the thermometer's constant (kPa/ $^\circ\text{C}$ ). For the daily evapotranspiration,  $G \approx 0$ . The value of  $u_2$  may be calculated by

$$u_2 = u_z \frac{4.87}{\ln(67.8Z - 5.42)} \quad (3)$$

where  $u_z$  is the measured wind speed at  $z$  m above ground. The value of  $e_s$  is calculated by

$$e_s = \frac{e^0(T_{\max}) + e^0(T_{\min})}{2} \quad (4a)$$

$$e^0(T) = 0.611 \exp\left[\frac{17.27T}{T + 237.3}\right] \quad (4b)$$

Values of  $\Delta$  and  $\gamma$  are calculated by

$$\Delta = \frac{4098 \left[ 0.6108 \exp\left(\frac{17.27T}{T + 237.3}\right) \right]}{(T + 237.3)^2} \quad (5a)$$

$$\gamma = 0.665 \times 10^{-3} P \quad (5b)$$

$$P = 101.3 \left( \frac{293 - 0.0065Z}{293} \right)^{5.26} \quad (5c)$$

where  $P$  is atmospheric pressure (kPa) and  $Z$  (m) is the local elevation, which is different in three different meteorological stations. The net radiation (i.e.  $R_n$ ) is calculated by the following equations:

$$R_n = R_{ns} - R_{nl} \quad (6a)$$

$$R_{ns} = (1 - \alpha) R_s \quad (6b)$$

$$R_{nl} = \sigma \left( \frac{T^4_{\max, k} + T^4_{\min, k}}{4} \right) (0.34 - 0.14\sqrt{ea}) \left( 1.35 \frac{R_s}{R_{so}} - 0.35 \right) \quad (6c)$$

$$R_s = \left( a_s + b_s \frac{n}{N} \right) \times R_a \quad (6d)$$

$$R_{so} = (0.6381 + 5.48 \times 10^{-5} \times Z) \times R_a \quad (6e)$$

where  $R_{ns}$  is the net longwave radiation,  $R_s$  is the solar radiation,  $R_a$  is the Zenith radiation ( $\text{MJ} \cdot \text{m}^{-2} \cdot \text{day}^{-1}$ ),  $\alpha = 0.23$ ,  $\sigma = 4.903 \times 10^{-9} \text{ MJ} \cdot \text{K}^{-4} \cdot \text{m}^{-2} \cdot \text{day}^{-1}$  is the Stefan-

Boltzmann constant,  $n$  is the actual duration of sunshine in a day (hour), and  $N$  is the maximum possible sunshine duration in a day (hour). The two coefficients in Equation 6(d), which are  $a_s = 0.24$  and  $b_s = 0.6$ , were adopted from Xie (2012). Both  $R_a$  and  $e_a$  were calculated following FAO 56.

With the knowledge of  $ET_0$ ,  $ET_a$  for each of the four LULC types may be calculated by

$$ET_{a,i} = ET_0 K_i \quad (7)$$

where the subscript  $i$  represents grassland, peatland, water body, and desertified land, respectively.  $K_i$  is the correction factor that is different for each LULC type and hence is determined separately.

### *The correction factor for grassland and peatland*

For either grassland or peatland, the correction factor ( $K_c$ ) accounts for the difference not only between the “reference crop” and various LULC types but also between vegetation canopy and air resistance (Allen et al., 1998). Its value varies with growth stages of vegetation, which may be divided into initial, rapid, middle, and late growth stages. Initial growth is denoted as the green plant from the appearance of green to the ground coverage of 10%, rapid growth prevails from the end of initial growth to full coverage of the ground, mid-growth lasts from rapid growth to plant maturity, and late growth is from ripening to plant withering (Allen et al., 1998).

Values of  $K_c$  at different growth stages were determined using the single-factor crop method (Allen et al., 1998), which couples the effects of crop transpiration and soil evaporation with  $K_c$ , such that only  $K_{c, ini}$ ,  $K_{c, mid}$ , and  $K_{c, end}$  need to be selected. Given that these variables are defined differently for different growth stages by the FAO56's *Drainage and Irrigation Handbook*, the selected initial crop coefficients  $K_{c, ini}$ ,  $K_{c, mid}$ , and  $K_{c, end}$  need to be corrected, and the FAO56 provides both the formula and the chart for selection. As  $K_{c, ini}$  is mainly affected by the soil moisture and atmospheric evaporation, it may be determined directly from the table in the FAO56. Values of  $K_{c, mid}$  and  $K_{c, end}$  were calculated using the following equations:

$$K_{c,mid} = K_{c,mid}(T) + [0.04(u_2 - 2) - 0.004(RH_{min}) - 45](h/3)^{0.3} \quad (8a)$$

$$K_{c,end} = K_{c,end}(T) + [0.04(u_2 - 2) - 0.004(RH_{min}) - 45](h/3)^{0.3} \quad (8b)$$

where,  $K_{c,mid}(T)$ ,  $K_{c,end}(T)$  may be found from the crop coefficient table of the FAO56,  $1 < u_2 < 6$  m/s,  $RH_{min}$  represents the mean value for daily minimum relative humidity during the growth stage and  $20\% \leq RH_{min} \leq 80\%$ ,  $h$  reflects the average height of crop at the growth phase and  $0.1 < h < 10$  m.

In the Zoige basin, the growth rate of vegetation is generally slow due to the prolonged winter with low temperatures. Therefore, the reference values provided by the FAO56 for  $u_2$ ,  $h$ , and  $RH_{min}$  could not be directly used to calculate  $K_c$  at different growth stages. By adjusting these values for the Zoige basin, the average and monthly values of  $K_c$  for each stage were finally estimated for the three stations of the study area (Tables 1 and 2).

**Table 1.** Values of  $K_c$  for different growth stages at the three stations.

	Grassland			Peatland		
	$K_{c,ini}$	$K_{c,mid}$	$K_{c,end}$	$K_{c,ini}$	$K_{c,mid}$	$K_{c,end}$
Zoige	0.4	0.750	0.596	0.7	1.108	0.628
Hongyuan	0.4	0.731	0.594	0.7	1.097	0.620
Maqu	0.4	0.730	0.595	0.7	1.093	0.622

**Table 2.** Monthly values of  $K_c$  for grassland and peatland.

Type	Station	15			1 July –		11		
		1 Jan. – 14 April	Apr. – 10-May	11–31 May	20 Sept.	21–30 Sept.	1–10 Oct.	31 Dec.	
grassland	Zoige	0.3	0.4	0.446	0.51	0.75	0.718	0.637	0.3
	Hongyuan	0.3	0.4	0.443	0.504	0.731	0.702	0.63	0.3
	Maqu	0.3	0.4	0.435	0.497	0.73	0.702	0.631	0.3
peatland	Zoige	0.4	0.7	0.755	0.830	1.108	1.007	0.754	0.4
	Hongyuan	0.4	0.7	0.745	0.820	1.097	0.997	0.746	0.4
	Maqu	0.4	0.7	0.727	0.804	1.093	0.994	0.746	0.4

### The correction factor for water body

Evaporation from a water body may only be measured using an evaporation pan ( $ET_p$ ), which means that  $ET_{a,w}$  in Equation (1) is equivalent to  $ET_p$ . In the study area, however, values of  $ET_p$  were merely available for 10 years within the 1967–2011 period in the Yellow River Hydrological Yearbook. Thus, the correction factor, denoted as  $K_p$ , is needed to calculate  $ET_p$  for other years of the same period. The earlier finding showed that  $ET_p$  is linearly related to  $ET_0$  (Xie, 2012). It follows that for the 10 years when  $ET_p$  were available, the ratio of  $ET_p$  to the associated  $ET_0$  may serve as the correction factor. Accordingly, the average of these ratios was used as  $K_p$ , which was 0.917, 0.898, and 0.879 for the Zoige, Hongyuan, and Maqu stations, respectively. Values of  $ET_p$  for other years of the 1967–2011 period were subsequently calculated using Equation (7).

**The correction factor for the desertified land.** The correction factor for the desertified land, denoted as  $K_d$ , was determined by referring the evaporation coefficient from an earlier study where it ranged between 0.13 and 0.20 for the grassland and desert in a semi-arid area (Li & Gao, 2004). Compared to that area, the Zoige basin is wetter due to its relatively high annual precipitation. Furthermore, the desertified land in the study area was caused by grassland degradation and thus may still have sparse vegetation cover. Consequently, the value of  $K_d$  was selected as 0.25. Although this value might not be sufficiently accurate, the small percentage of desertified land in the total area suggests that the uncertainty in the determination of  $K_d$  should not affect the calculation of the actual evapotranspiration (i.e. Equation (1)).

## Results and analysis

### Area changes of LULC types in 1990-2016

On average, grassland and peatland were the dominant LULC types in the Zoige basin, covering 79.89% and 18.69% of the total area, respectively. Water body only covered

about 0.87%, followed by forested, desertified, and construction lands, taking 0.28%, 0.20%, and 0.08%, respectively. From 1990 to 2016, the area of grassland continuously increased, following a roughly linear trend with the average increase rate of  $66.76 \text{ km}^2/\text{yr}$  (Figure 3). On the contrary, the area of peatland decreased since 1990 at the rate of  $66.54 \text{ km}^2/\text{yr}$ . This reduction has been attributed to both human and natural factors, including ditch excavation, headward erosion of gullies, and peat desiccation (Bai, Lu, Zhao, Wang, & Ouyang, 2013; Li et al., 2015, 2014; Zhang et al., 2014). The nearly equal rates of change in the two LULC types suggests that most of the decreased peatland might have been turned into grassland.

Although forest, construction, and desertified lands together occupied a very small proportion (i.e. 0.58%) of the total area, they still experienced temporal variations. Forest land, mainly distributed in the western Zoige basin among a series of mountain belts (i.e. Minshan Mountains), decreased over the entire period, with two short periods (i.e. 1995–1998 and 2008–2010) of increase (Figure 3). Local logging and construction timber might be the main reasons for forest area reduction. It is also possible that the

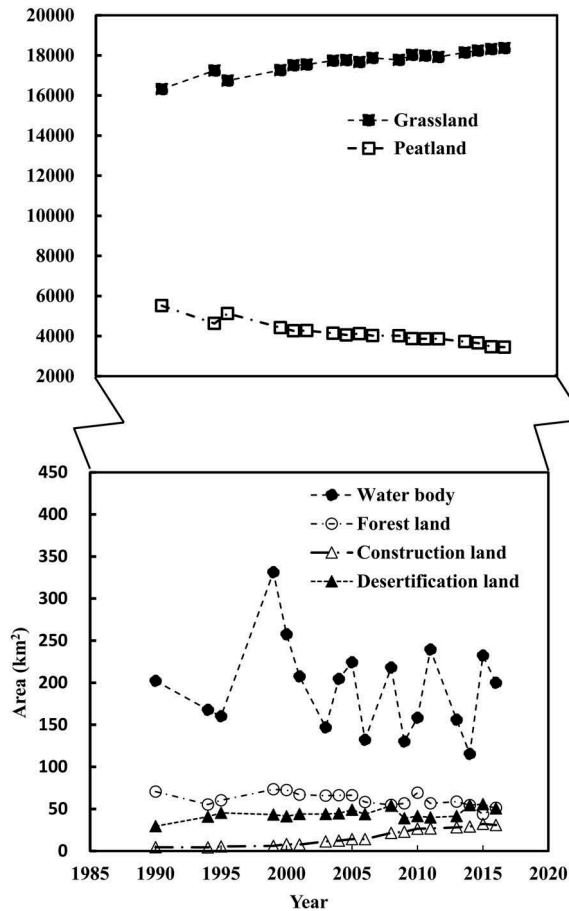


**Figure 3.** Areas of grassland, peatland, water body, forestland, construction, and desertification land between 1990 and 2016.

increases might be partially caused by errors arisen from image processing. Nonetheless, these potential errors would not affect the increase trend because the forestland cover only a very small proportion of the total area. While occupying an almost negligible percentage of the total area, the actual area of construction land increased nearly seven times from 1990 to 2016, indicating the increase of population and expanded urbanization in the Zoige basin, which has been reported in many studies (Hu et al., 2012; Xiao, Tian, Tian, & Yang, 2010; Yan & Wu, 2005; Yang et al., 2017). The desertified land also increased during the entire period, from 29.51 in 1990 to 50.77 km<sup>2</sup> in 2016 (Table 5). Our field observation showed that desertified lands, which are sporadically distributed in the Zoige basin, may be caused by either natural processes or overgrazing (Hu et al., 2012, 2018; Yu et al., 2017). Those caused by the former tend to occur on locally steep ground, whereas the others typically lie along roads. While exactly how natural processes cause desertification is still not clear, the lower rate of increase of desertified land from 1990 to 2016, (~72%) suggests that climate change and anthropogenic activities might have limited impact on desertification in the Zoige basin.

The area occupied by water bodies was greater than the sum of forest, construction, and desertified lands, though it was still less than 1% of the total. From 1990 to 2016, this area oscillated between 115 and 258 km<sup>2</sup> (Figure 3). The oscillation pattern of temporal changes of water bodies clearly reflected the strong influence of variable annual precipitation, which will be described later. Overall, temporal changes of LULC types in the Zoige basin were mainly controlled by those of grassland and peatland.

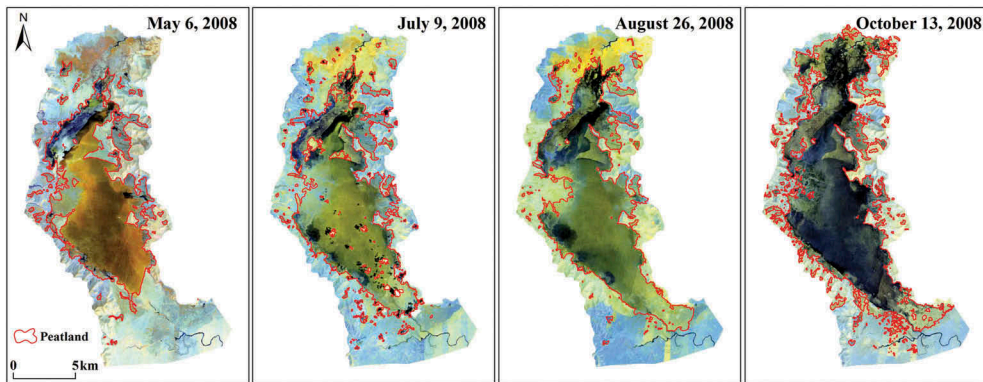
### *Impact of specific cumulative precipitation on calculation of peatland area*

The specific cumulative precipitation (SCP) was generally higher at the Hongyuan station than that of the other two stations (Table 3), indicating a spatial trend of precipitation in the Zoige basin. Comparing the spatially weighted mean with the simple arithmetic mean showed that their differences were negligible (between almost 0% and 2%) and thus the latter was used in this study (Table 3). Values of SCP ending in July and August took about 43–62% of the associated annual precipitation (AP). The percentage went up to 77–82% for those ending in September. These percentages indicated that SCP values ending before October were quite different from the corresponding AP values. Given that most satellite images were obtained before or in early October (Table 3), SCP rather than AP should be more relevant to the status of peatland swamps and hence affect the area extracted from the images.

This effect was illustrated in an example that showed variable peatland areas, extracted using the method described previously, from May to October 2008 in a small area of the Zoige basin (33° 35' 14" N, 102° 05' 38" E) (Figure 4). Different SCP values in the four months led to different sizes of peatland swamps. Also, different growth rates of vegetation on peatland affected the identification of dry peatland. Both factors worked together to cause the change of the identified peatland areas in these four months. While there was only one AP value for the year, each month was associated with a different SCP value, and these values were highly correlated with peatland areas (Figure 5). Therefore, peatland areas extracted from multi-year images

**Table 3.** Annual and specific cumulative precipitation between 1990 and 2016.

Cumulative Date	Cumulative precipitation (mm)				Annual precipitation (mm)	Ratio of cumulative precipitation (%)
	Maqu	Zoige	Hongyuan	Average		
July 8,1990	227	279.4	303.9	270.1	625.4	43.2
August 4,1994	361.8	373.7	445.9	393.8	630.4	62.5
4 August 1995	329.3	362.4	509.2	400.3	650.9	61.5
December 14,1999	637.7	600.8	918.1	718.9	725.1	99.1
31 October 2000	507.3	575.5	718.0	600.3	615.3	97.6
15 August 2001	373.8	334.1	421.0	376.3	648.6	58.0
14 September 2003	623.0	615.2	638.2	625.5	763.3	81.9
16 September 2004	494.9	543.1	474.6	504.2	625.2	80.6
16 September 2005	515.2	504.5	657.5	559.1	728.2	76.8
5 August 2006	269.7	287.8	342.9	300.1	586.0	51.2
13 October 2008	512.3	420.7	600.4	511.1	550.0	92.9
28 July 2009	390.6	294.7	496.3	393.9	670.2	58.8
6 October 2010	532.2	808.9	707.6	682.9	733.4	93.1
6 October 2011	579.0	629.8	675.2	628.0	693.3	90.6

**Figure 4.** Identified peatland extents (bounded by red lines) in different months of 2008 from a small area within the Zoige basin.

obtained in different months of a year need to be corrected for inter-month variations before used for further analysis.

### **Characteristics of $ET_a$ for the four LULC types**

Physical and physiological features of the four LULC types with respect to the actual annual evapotranspiration rate were reflected by their calculated  $ET_a$  values. During the 1967–2011 period, the mean annual  $ET_a$  of water bodies was 805.80 mm, followed by 667.98 mm for peatland (Table 4). That of the grassland and forestland was even less, with the value of 447.18 mm, and the desertified land was only 224.40 mm (Table 4). These values indicated that if the Zoige basin were solely covered by each of the four LULC types, then the annual evapotranspiration rate would be highest for water body, which would be followed by peatland, grassland and forestland, and desertified land. Despite these differences, the annual  $ET_a$  for all LULC types shared a similar degree of

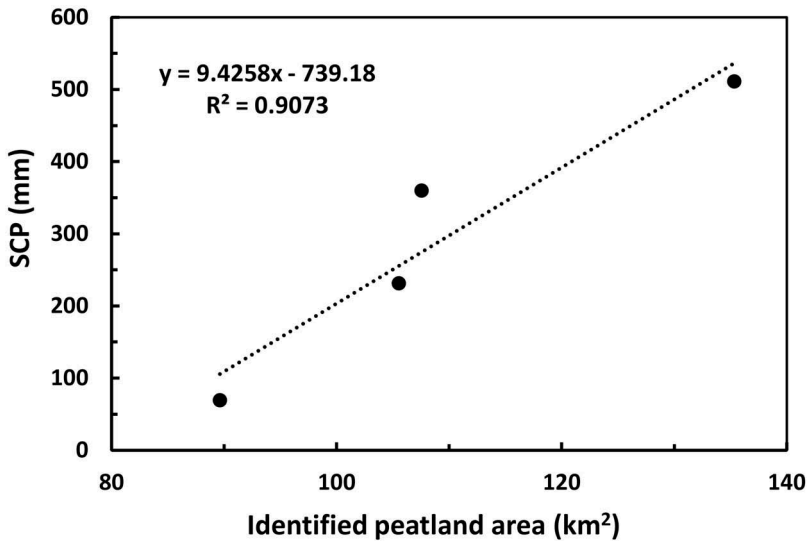


**Figure 5.** Peatland area versus the associated SCPs in four different months of 2008. The dashed line was the regression line between the two variables.

**Table 4.** Statistical summary of  $ET_a$  (mm yr<sup>-1</sup>) for the four LULC types during the 1967–2011 period.

	Water body	Peatland	Grassland & forest land	Desertification land
Mean	805.8	668.0	447.2	224.4
St. Dev	28.22	24.04	16.10	7.86
CV*	0.035	0.036	0.036	0.035

\*CV is coefficient of variation.

variation over the 1967–2011 period, which was evidenced by similar CV values (Table 4).

Nonetheless, the actual evapotranspiration rate in the Zoige basin is a cumulative effect of all LULC types over their spatial extents, which may be represented by the area weighted  $ET_a$  value for each LULC type. Calculation of these values (Figure 6) produced a different order of actual evapotranspiration rates among the four LULC types compared with the earlier results. Grassland made the highest contribution to the total annual evapotranspiration rate, with ~74%, whereas peatland was the second with ~24% of the total. That from water body only contributed ~1.8%, clearly reflecting the consequence of the much smaller area of water body in the Zoige basin. The even smaller area of the desertified land (Figure 3) made its evapotranspiration negligible (Figure 6).

The degrees of variation of area-weighted  $ET_a$  values for the four LULC types still remained similar, as indicated by their similar CV values (between 0.035 and 0.036). This similarity suggests that considering spatial variability of the annual evapotranspiration rates for all LULC types did not change their temporal patterns. Furthermore, linear regression models established between the area-weighted  $ET_a$  for all LULC types and time (year) were statistically insignificant, signifying that the area-weighted  $ET_a$

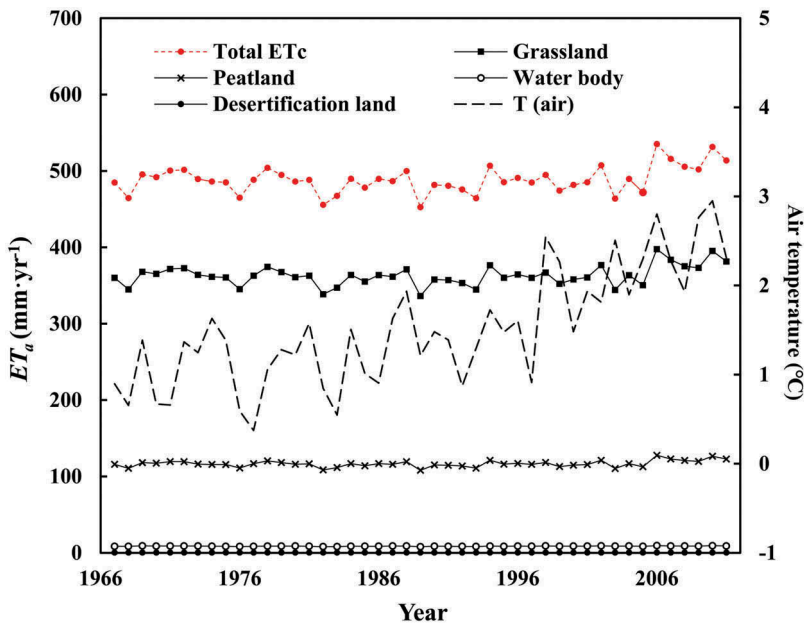


**Figure 6.** Area-weighted  $ET_a$  values for the four LULC types and total  $ET_a$  during the 1967–2011 period.

values generally did not follow any temporal trend during the 1967–2011 period, though they clearly increased after 2000 (Figure 6). These temporal trends were clearly related to those of air temperature. Despite its higher degree of variation ( $CV = 0.43$ ), the air temperature showed a similar temporal pattern to that of the area weighted  $ET_a$  values (Figure 6). In addition, its general increasing rate during the 1967–2011 period was accelerated since 2000. Thus, air temperature and its temporal variation are the essential factors controlling the changes of actual evapotranspiration, which marginally suggests that the  $ET_a$  values determined using the method developed in this study are reasonable. Nonetheless, the temporal trends of these values (Figure 6) were at odds with the continuously decreasing trend of peatland area. Apparently, changes of actual evapotranspiration alone are incapable of explaining the cause of peatland reduction.

## Discussion

### *Uncertainties in data analysis*

In this study, the spatially distributed  $P$  and  $E$  values in the Zoige basin were determined from the kriging analysis based on the original data obtained from three weather stations within the study area (Figure 1). The limited number of weather stations could raise concerns about the accuracy of the calculated  $P$  and  $E$  values. Although not able to change this fact, we assessed the uncertainties possibly involved in these values from three different perspectives using  $P$  values as an example. The first tested the potential impact of adopting different interpolation methods. Using daily data from 1990 and 2008, which were selected randomly, we performed a different interpolation analysis

(i.e. the Inverse Distance Weight (IDW) method) to calculate spatial distribution of  $P$  values. Comparison of the mean  $P$  across the study area with that generated using the Kriging method showed that the possible difference in calculating  $P$  values using two different methods merely gave rise to <1% of variation in the calculated mean  $P$  values for both 1990 and 2008. Obviously, utilizing different interpolation methods would not cause significant difference in the calculated mean annual  $P$  values and hence has negligible effect on the reported results.

The second examined the potential influence of including more weather stations outside of the study area. By adding the data from two nearest weather stations outside of the study area to the original ones (Figure 7) and repeating interpolation analysis, we found that the difference in calculated mean  $P$  values from 1990 was 1.46% and 1.51% for the Kriging and IDW methods, respectively, while that for the 2008 data was 4.08% and 3.69% for the two interpolation methods, respectively. Therefore, adding data from weather stations outside of the study area will not improve the accuracy of the calculated mean  $P$  values.

The third evaluated the possible influence of orographic precipitation due to topography. The study area contains two mountain/hill clusters with areas of 729.16 (part 1) and 1200.52 km<sup>2</sup> (part 2) (Figure 7). The grassland area within the two parts covers about 10%, while peatland covers only about 1.2% of the total area. Even if the orographic precipitation may cause some errors in calculated mean  $P$  values, these

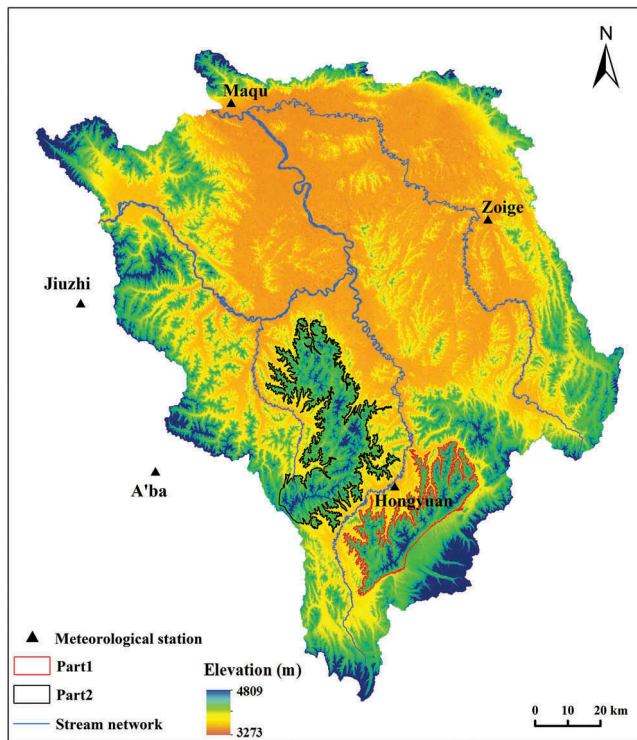


**Figure 7.** Design of error estimation. The two weather stations outside of the study area are the nearest ones. Parts 1 and 2 are the two clusters that include local hills and mountains.

possible errors would at most affect about 10% and 1.2% of grassland and peatland, respectively. Thus, our argument about the linkage between  $P$  (and  $E$ ) and peatland areas should not be affected by these possible errors. Overall, these assessments indicated that our analysis was robust, despite limited data.

### **Peatland area and precipitation**

The relationship shown in Figure 5 suggested that the identified peatland area in different days of a given year may be linearly related to the SCPs up to these different days. To develop a method of eliminating the incomparable peatland areas obtained from satellite imagery taken at different times in different years (Bai, Lu, Wang, et al., 2013; Jiang et al., 2017; Li et al., 2011; Xiao et al., 2010; Yu et al., 2017; Zhang et al., 2016), we calculated peatland areas in May, August, and October 2008 using available satellite images and the associated SCP values of the same year. Using these data, we established a linear model between peatland area ( $A$ ) and SCP with  $R^2 = 0.817$  and  $p < 0.01$ , which subsequently led to a correction method for peatland areas identified from different months of a given year:

$$\Delta A = 1.1636 \times \Delta \text{SCP} \quad (9)$$

where  $\Delta \text{SCP}$  is the change of SCP values from one date to another within a year and  $\Delta A$  is the change of peatland areas between the two different dates. Since Equation (9) was based on the only four monthly images available in 2008, it needs to be verified when more images in different years are available. Yet, it provided a practical tool to correct at the first approximation such uncertainty in determining the peatland area.

Based on Equation (9), the originally identified peatland areas of 14 years in the 1990–2016 period (Table 3) were corrected by converting them into the areas equivalent to the one obtained on 8 July 1990 (Figure 8). The correction indicated that the inconsistency among the dates of these images caused general over-estimation of the peatland areas because all dates of the images after 1990 were later than 8 July (Table 3). Depending on the value of SCP, the peatland area may be over-estimated by as much as 10.5% (1999) and as little as 1.2% (1994). Corrected peatland areas followed a decreasing linear trend with statistical significance ( $p < 0.01$ ) and the mean annual reduction rate was  $81.0 \text{ km}^2/\text{yr}$  from 1990 to 2016, which was higher than that based on the original areas (i.e.  $71.4 \text{ km}^2/\text{yr}$ ).

SCP values on 8 July for the 14 years listed in Table 3 should be most relevant to the change of peatland areas of the same 14 years. Unfortunately, the former showed no clear trend, with an undulated pattern in the 14 years (Figure 8). This pattern was inconsistent with the decreasing trend of peatland area for the same period. Therefore, cumulative precipitation alone was insufficient to explain the reduction of peatland area.

### **Coupled impact of SCP and evapotranspiration on peatland reduction**

Our calculation indicated that the total  $ET_a$  in the Zoige basin was between 450 and 550 mm (Figure 6). This result was slightly higher than the previous estimate, which

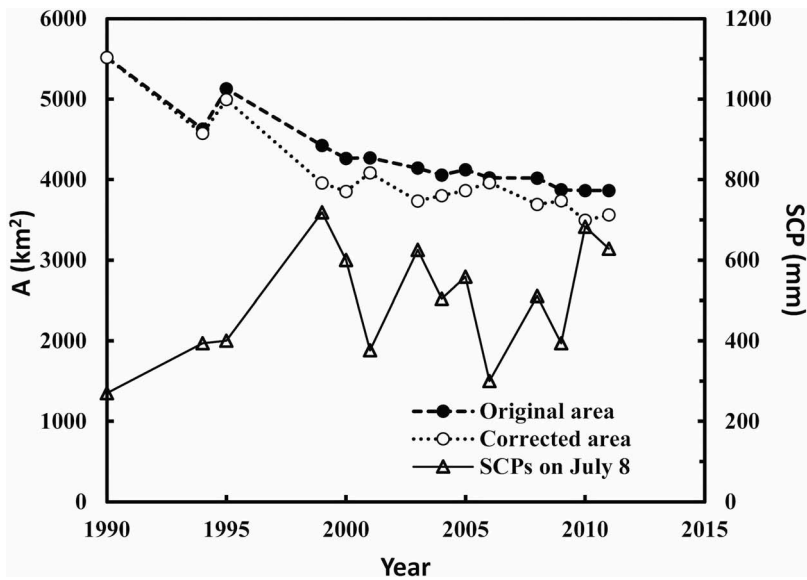


**Figure 8.** Original and corrected peatland areas and associated SCP values from 1990 to 2016. The correction was based on 8 July 1994 of the earliest image and achieved using Eq. (9).

ranged between 300 and 500 mm (Yin, Wu, Zhao, Zheng, & Pan, 2012). The discrepancy may be attributed to many factors, including use of different methods for selecting the  $K$  value (Xie, 2012) and the argument that the P-M method is inappropriate for estimating  $ET_a$  in the Qinghai–Tibet Plateau (Wang, Zhang, Wang, & He, 2016). Our results led to the belief that though the original FAO56 P-M formula was derived for calculating evapotranspiration from the flat, cropped neat farmland located in low-altitude plains, our modified method, which included Equations (1–7) and different ways of selecting the  $K$  values for different LULC types, was sufficient to distinguish different evapotranspiration rates among different LULC types and to appropriately determine the actual annual evapotranspiration rate.

Early studies showed that evapotranspiration for a single vegetation type increased at the rate ranging between 0.755 and 1 mm/yr for the past few decades and treated this increase as the cause of peatland degradation (Li et al., 2014; Zhang et al., 2016). Yet, our results indicated that this rate did not change significantly in the 1967–2011 period, though from 2000 to 2011, it generally increased at a much higher rate, of 3.744 mm/yr (Figure 6). Apparently, neither SCP nor  $ET_a$  may explain the temporal trend of area reduction. It is thus necessary to explore their coupled effect, which may be represented by a new dimensionless index, RPE, calculated as the ratio of SCP to evapotranspiration. RPE correctly reflected their opposite effects on the change of the peatland area, and its temporal changes were examined in two ways. First, we calculated daily RPE values in 1970, 1990, and 2010 to represent three different stages of the 1967–2011 period and plotted these values against days in one year (Figure 9(a)). Second, we calculated three types of annual RPE values during the 1967–2011 period, in which SCP values ended on 31 August 1931 October, and 31 December, respectively (Figure 9 (b)). In all three selected years, daily RPE values followed a similar convex upward

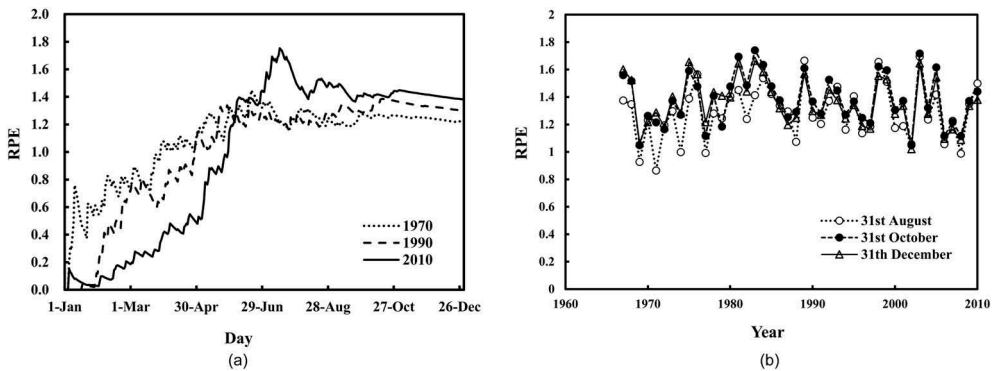


**Figure 9.** Temporal trends of the RPE values. (a) daily cumulative curves of the RPE values in three selected years; (b) annual changes of the RPE values based on SCP accumulated to August, October, and December, respectively.

curve. Before 30 April, RPE values were all  $<1$ , indicating that precipitation was less than evapotranspiration in winter and spring, though the magnitude of the latter was indeed low (Figure 6). The curve generally increased from May to October with different degrees of variation in different years, which may primarily reflect the variation of summer SCP. During this period of a year, the RPE values, which were all  $>1$ , suggested that though evapotranspiration was high due to high air temperature, precipitation also increased and its increasing rate was higher than that of evapotranspiration. From late October to the end of a year, the curve decreased marginally with the RPE values still  $>1$ . This pattern revealed that though evapotranspiration may be higher than precipitation on individual days, represented by locally decreasing sections in Figure 9a, cumulative precipitation was always greater than the associated total evapotranspiration in the three selected years. It should be noted that compared to the curves for 1970 and 1990, the curve in 2010 was much lower before May, much higher between May and September, and generally higher from September to December. This inter-annual difference suggested that more 2010 precipitation occurred during summer than in winter and spring.

Examining the temporal trend of the RPE values for the entire period (i.e. 1967–2011) (Figure 8(b)) signified that they were all  $>1$  except five years ending at 31 August (i.e. 1969, 1971, 1974, 1977, and 2008). This meant that the cumulative precipitation generally contributed more than evapotranspiration to peatland hydrological processes of Zoige basin. Although these temporal trends showed a decreasing tendency (Figure 9(b)), linear regression analysis indicated that not only the decreasing rate was very low (0.021/yr), but also the linear trend was not statistically significant. During the 1967–2011 period, the curves were characterized by a serrated pattern, indicating that RPE could either increase or decrease by 100% from one year to another. The implication was that the temporal change of RPE values was mainly characterized by their oscillations over the years. Thus, evapotranspiration is unlikely the key factor causing the continuous area reduction of peatland. It appears that excavated artificial ditches and development of natural gullies might play a significant role in peatland degradation by draining water out of peatland (Li et al., 2015;

Li et al., 2018; Li & Gao, 2019; Zhang et al., 2014), though further process-based studies on short-term hydrological processes are needed to verify this role.

## Conclusions

Using daily meteorological and precipitation data downloaded from three local stations and satellite imagery from the 1967–2011 period in the Zoige basin, China, we investigated uncertainties in identifying peatland areas using Landsat imagery; determined different rates of evapotranspiration (ET) from different LULC types by considering the variable effects on ET from different LULC types, and revealed temporal patterns of the interaction between precipitation and ET. We found that the identified peatland area from a given satellite image was strongly affected by the specific cumulative precipitation (SCP), such that peatland areas identified in different months of the same year may be significantly different. Thus, peatland areas extracted from the images in different years may not be directly comparable because they were not taken in the same month of these years. This uncertainty may be reduced by converting the peatland areas identified in different months of multiple years to those of the same month using the linear relation developed in Equation (9). Based on a modified P-M equation that differentiated different ET rates from the four LULC types, we showed that in the Zoige basin, LULC types that may produce ET rates were, in descending order, water body, grassland and forestland, peatland, and desertified land. When the area-weighted ET rate was calculated, grassland may generate the highest rate, followed by peatland and other LULC types, suggesting that ET is primarily contributed from grassland and peatland. Total annual ET was between 450 and 550 mm, which was higher than that from the previous studies. The fact that the ratio of SCP to evapotranspiration (RPE) began to be  $>1$  from May of a year and the annual RPE was generally  $>1$  during the 1967–2011 period suggested that though ET has increased due to global warming, the associated SCP was always greater than ET. Therefore, the continuous reduction of peatland area cannot be solely ascribed to climate change. The dewatering effect caused by artificial ditches and natural gullies in the Zoige basin might be a significant factor, but needs to be further confirmed by future studies.

## Acknowledgments

The corresponding author was also partially supported by the Appleby-Mosher fund of Maxwell School of Citizenship and Public Affairs, Syracuse University. We thank Meng Sun for partially data processing and three anonymous reviewers for constructive comments and suggestions.

## Disclosure statement

No potential conflict of interest was reported by the authors.

## Funding

This work was supported by the Open Project of State Key Laboratory of Plateau Ecology and Agriculture, Qinghai University [2017-KF-01], National Natural Science Foundation of China [51622901, 91647204, 51709020], Project of Qinghai Science & Technology Department [2016-ZJ-Y01], and Overseas Expertise Introduction Project for Discipline Innovation [D18013], and Open Research Fund Program of State Key Laboratory of Hydroscience and Engineering (sklhe-2019-A03).

## ORCID

Zhiwei Li  <http://orcid.org/0000-0002-2870-7265>

## References

- Abtew, W., Obeysekera, J., & Iricanin, N. (2011). Pan evaporation and potential evapotranspiration trends in South Florida. *Hydrological Processes*, 25(6), 958–969.
- Allen, R. G., Pereira, L. S., Raes, D., & Smith, M. (1998). *Crop evapotranspiration\_ guidelines for computing crop water requirements- FAO Irrigation and drainage paper 56*. Rome: FAO - Food and Agriculture Organization of the United Nations.
- Bai, J., Hua, O., Cui, B., Wang, Q., & Chen, U. (2008). Changes in landscape pattern of alpine wetlands on the Zoige Plateau in the past four decades. *Acta Ecologica Sinica*, 28(5), 2245–2252.
- Bai, J., Lu, Q., Wang, J., Zhao, Q., Ouyang, H., Deng, W., & Li, A. (2013). Landscape pattern evolution processes of alpine wetlands and their driving factors in the Zoige Plateau of China. *Journal of Mountain Science*, 10(1), 54–67.
- Bai, J., Lu, Q., Zhao, Q., Wang, J., & Ouyang, H. (2013). Effects of alpine wetland landscapes on regional climate on the Zoige Plateau of China. *Advances in Meteorology*, (2013), 1–7.
- Bian, J., Li, A., & Deng, W. (2010). Estimation and analysis of net primary productivity of Ruoergai wetland in China for the recent 10 years based on remote sensing. *Procedia Environmental Sciences*, 2, 288–301.
- Carlson Mazur, M. L., Wiley, M. J., & Wilcox, D. A. (2014). Estimating evapotranspiration and groundwater flow from water-table fluctuations for a general wetland scenario. *Ecohydrology*, 7(2), 378–390.
- Clinton, N., Holt, A., Scarborough, J., Yan, L., & Gong, P. (2010). Accuracy assessment measures for object-based image segmentation goodness. *Photogrammetric Engineering & Remote Sensing*, 76(3), 289–299.
- Cui, M., Ma, A., Qi, H., Zhuang, X., Zhuang, G., & Zhao, G. (2015). Warmer temperature accelerates methane emissions from the Zoige wetland on the Tibetan Plateau without changing methanogenic community composition. *Scientific Reports*, 5, 11616.
- Fan, S. (1988). Applications of remote-sensing techniques in peat resource investigations in Zoige. *Acta Geologica Sinica*, 1(1), 101–112.
- Gao, J. (2006). Degradation factor analysis and solutions of Ruoergai wetland in Sichuan. *Sichuan Environment*, 25(4), in Chinese, 48–52.
- Glenn, E. P., Mexicano, L., Garcia-Hernandez, J., Nagler, P. L., Gomez-Sapiens, M. M., Tang, D., ... Zamora-Arroyo, F. (2013). Evapotranspiration and water balance of an anthropogenic coastal desert wetland: Responses to fire, inflows and salinities. *Ecological Engineering*, 59, 176–184.
- Gong, P., Niu, Z., Cheng, X., Zhao, K., Zhou, D., Guo, J., ... Yan, J. (2010). China's wetland change (1990–2000) determined by remote sensing. *Science China Earth Sciences*, 53(7), 1036–1042.
- Guo, J., & Li, G. (2007). Climate change in Zoige Plateau marsh wetland and its impact on wetland degradation. *Plateau Meteorology*, 26(2), 422–428.

- Hu, G., Dong, Z., Lu, J., & Yan, C. (2012). Driving forces of land use and land cover change (LUCC) in the Zoige Wetland, Qinghai-Tibetan Plateau. *Sciences in Cold and Arid Regions*, 4(5), 422.
- Hu, G., Dong, Z., Lu, J., & Yan, C. (2015). The developmental trend and influencing factors of aeolian desertification in the Zoige Basin, Eastern Qinghai-Tibet Plateau. *Aeolian Research*, 19, 275–281.
- Hu, G., Yu, L., Dong, Z., Lu, J., Li, J., Wang, Y., & Lai, Z. (2018). Holocene aeolian activity in the Zoige Basin, northeastern Tibetan Plateau, China. *Catena*, 160, 321–328.
- Hu, Y., Maskey, S., & Uhlenbrook, S. (2011). Trends in temperature and rainfall extremes in the Yellow River source region, China. *Climatic Change*, 110(1–2), 403–429.
- Jacobs, J. M., Mergelsberg, S. L., Lopera, A. F., & Myers, D. A. (2002). Evapotranspiration from a wet prairie wetland under drought conditions: Paynes prairie preserve, Florida, USA. *Wetlands*, 22(2), 374–385.
- Jiang, W., Lv, J., Wang, C., Chen, Z., & Liu, Y. (2017). Marsh wetland degradation risk assessment and change analysis: A case study in the Zoige Plateau, China. *Ecological Indicators*, 82, 316–326.
- Li, B., Yu, Z., Liang, Z., Song, K., Li, H., Wang, Y., ... Acharya, K. (2014). Effects of climate variations and human activities on runoff in the Zoige alpine wetland in the eastern Edge of the Tibetan Plateau. *Journal of Hydrologic Engineering*, 19(5), 1026–1035.
- Li, C., & Gao, S. (2004). Study on the moisture budget of the grasslands in the semiarid regions in north China. *Arid Zone Research*, 21(4), 338–342. (in Chinese with English abstract).
- Li, J., Erickson, J. E., Peresta, G., & Drake, B. G. (2010). Evapotranspiration and water use efficiency in a Chesapeake Bay wetland under carbon dioxide enrichment. *Global Change Biology*, 16(1), 234–245.
- Li, L., Hao, Z., Wang, J., Wang, Z., & Yu, Z. (2008). Impact of future climate change on runoff in the Head region of the Yellow River. *Journal of Hydrologic Engineering*, 13(1), 347–354.
- Li, Y., Zhao, Y., Gao, S., Sun, J., & Li, F. (2011). The peatland area change in past 20 years in the Zoige Basin, eastern Tibetan Plateau. *Frontiers of Earth Science*, 5(3), 271–275.
- Li, Z., & Gao, P. (2019). Impact of natural gullies on groundwater hydrology in Zoige peatland, China. *Journal of Hydrology*, 21, 25–39.
- Li, Z., Gao, P., & You, Y. (2018). Characterizing hydrological connectivity of artificial ditches in Zoige peatlands of Qinghai-Tibet plateau. *Water*, 10, 1364.
- Li, Z., Liu, X., Ma, T., Kejia, D., Zhou, Q., Yao, B., & Niu, T. (2013). Retrieval of the surface evapotranspiration patterns in the alpine grassland-Wetland ecosystem applying SEBAL model in the source region of the Yellow River, China. *Ecological Modelling*, 270, 64–75.
- Li, Z., Wang, Z., Brierley, G., Nicoll, T., Pan, B., & Li, Y. (2015). Shrinkage of the Ruorgai Swamp and changes to landscape connectivity, Qinghai-Tibet Plateau. *Catena*, 126, 155–163.
- Li, Z., Wang, Z., & Pan, B. (2016). Wetland ecosystems of the yellow river source zone. In Brierley, G., Li, X., Cullum, C. and Gao, J. (Eds.), *Landscape and ecosystem diversity, dynamics and management in the yellow river source zone* (pp. 183–207). Cham, Switzerland: Springer International Publishing AG.
- Liu, J., Chen, C., Qing, N., Li, X., Lai, J., & Guo, B. (2016). Response of water resources to climate change in Zoige, Tibetan Plateau. *Journal of Glaciology and Geocryology*, 38(2), 498–508.
- Lott, R. B., & Hunt, R. J. (2001). Estimating evapotranspiration in natural and constructed wetlands. *Wetlands*, 21(4), 614–628.
- Mao, L. M., Bergman, M. J., & Tai, C. C. (2002). Evapotranspiration measurement and estimation of three wetland environments in the Upper St. Johns River Basin, Florida. *Journal of the American Water Resources Association*, 38(5), 1271–1285.
- Mitra, S., Wassmann, R., & Vlek, L. G. P. (2005). An appraisal of global wetland area and its organic carbon stock. *Current Science*, 88(1), 25–35.
- Mitsch, W. J., Bernal, B., Nahlik, A. M., Ulo, M., Li, Z., Anderson, C. J., ... Brix, H. (2013). Wetlands, carbon, and climate change. *Landscape Ecology*, 28, 583–597.
- Mitsch, W. J., & Gosselink, J. G. (2015). *Wetlands* (Fifth ed.). Hoboken, New Jersey: John Wiley & Sons, Inc.

- Neubert, M., & Herold, H. (2008). Assessment of remote sensing image segmentation quality. *Proceedings GEOBIA 2018*, Calgary, Canada.
- Niu, Z., Zhang, H., Wang, X., Yao, W., Zhou, D., Zhao, K., ... Gong, P. (2012). Mapping wetland changes in China between 1978 and 2008. *Chinese Science Bulletin*, 57(22), 2813–2823.
- Raddatz, R. L., Papakyriakou, T. N., Swystun, K. A., & Tenuta, M. (2009). Evapotranspiration from a wetland tundra sedge fen: Surface resistance of peat for land-surface schemes. *Agricultural and Forest Meteorology*, 149(5), 851–861.
- Sica, Y. V., Quintana, R. D., Radeloff, V. C., & Gavier-Pizarro, G. I. (2016). Wetland loss due to land use change in the Lower Parana River Delta, Argentina. *Science of the Total Environment*, 568, 967–978.
- Song, K., Wang, Z., Du, J., Liu, L., Zeng, L., & Ren, C. (2014). Wetland Degradation: Its Driving Forces and Environmental impacts in the Sanjiang Plain, China. *Environmental Management*, 54(2), 255–271.
- Sprengrer, M., Tetazlaff, D., Tunaley, C., Dick, J., & Soulsby, C. (2017). Evaporation fractionation in a peatland drainage network affects stream water isotope composition. *Water Resources Research*, 53, 851–866.
- Sun, G. Y. (1992). A study on the mineral formation law, classification and reserves of the peat in the Ruergai plateau. *Journal of Natural Resources*, 7(4), 334–346. (in Chinese with English abstract)
- Sun, Z., Wei, B., Su, W., Shen, W., Wang, C., You, D., & Liu, Z. (2011). Evapotranspiration estimation based on the SEBAL model in the Nansi Lake Wetland of China. *Mathematical and Computer Modelling*, 54(3–4), 1086–1092.
- Tan, Y., Wang, X., Li, C., Cai, Y., Yang, Z., & Wang, Y. (2011). Estimation of ecological flow requirement in Zoige Alpine Wetland of southwest China. *Environmental Earth Sciences*, 66(5), 1525–1533.
- Wang, J., Wang, S., & Wang, Z. (2015). The variety characters of potential evapotranspiration and soil surface humidity index in the Zoige wetland in 1971–2010. *Scientia Geographica Sinica*, 35(2), 245–250.
- Wang, M., Yang, G., Gao, Y., Chen, H., Wu, N., Peng, C., ... Zhang, Y. (2015). Higher recent peat C accumulation than that during the Holocene on the Zoige Plateau. *Quaternary Science Reviews*, 114, 116–125.
- Wang, W., Xing, W., Shao, Q., Yu, Z., Peng, S., Yang, T., ... Singh, V. P. (2013). Changes in reference evapotranspiration across the Tibetan Plateau: Observations and future projections based on statistical downscaling. *Journal of Geophysical Research*, 118(10), 4049–4068.
- Wang, Z. F., Zhang, L. H., Wang, Y. B., & He, C. S. (2016). Diurnal variations of grassland evapotranspiration over different periods in the Pailugou basin in the upper reach of the Heihe River. *Chinese Journal of Applied Ecology*, 27(11), 3495–3504.
- Wossenu, A. (1996). Evapotranspiration measurements and modeling for three wetland systems in South Florida. *Water Resources Bulletin*, 32(3), 465–473.
- Xiang, S., Guo, R., Wu, N., & Sun, S. (2009). Current status and future prospects of Zoige Marsh in Eastern Qinghai-Tibet Plateau. *Ecological Engineering*, 35(4), 553–562.
- Xiao, D., Tian, B., Tian, K., & Yang, Y. (2010). Landscape patterns and their changes in Sichuan Ruergai Wetland National Nature Reserve. *Acta Ecologica Sinica*, 30(1), 27–32.
- Xie, H. (2012). *Evapotranspiration in Qing-Tibet Plateau and its response to climate change in 1970-2010*. (Ph.D.), Lanzhou University. (in Chinese).
- Yan, Z., & Wu, N. (2005). Rangeland privatization and its impacts on the Zoige wetlands on the Eastern Tibetan Plateau. *Journal of Mountain Science*, 2(2), 105–115.
- Yang, G., Peng, C., Chen, H., Dong, F., Wu, N., Yang, Y., ... Zhu, Q. (2017). Qinghai-Tibetan Plateau peatland sustainable. *Ecosystem Health and Sustainability*, 3(3). e01263. doi:10.1002/ehs2.1263
- Yao, W., Han, M., & Xu, S. (2010). Estimating the regional evapotranspiration in Zhalong wetland with the Two-Source Energy Balance (TSEB) model and Landsat7/ETM+ images. *Ecological Informatics*, 5(5), 348–358.

- Yin, Y., Wu, S., Zhao, D., Zheng, D., & Pan, T. (2012). Impact of Climate Change on Actual Evapotranspiration on the Tibetan Plateau during 1981-2010. *Acta Geographica Sinica*, 67(11), 1471–1481.
- Yu, K., Lehmkuhl, F., & Falk, D. (2017). Quantifying land degradation in the Zoige Basin, NE Tibetan Plateau using satellite remote sensing data. *Journal of Mountain Science*, 14(1), 77–93.
- Zhang, W., Lu, Q., Song, K., Qin, G., Wang, Y., Wang, X., ... Li, H. (2014). Remotely sensing the ecological influences of ditches in Zoige Peatland, eastern Tibetan Plateau. *International Journal of Remote Sensing*, 35(13), 5186–5197.
- Zhang, W., Yi, Y., Song, K., Kimball, J., & Lu, Q. (2016). Hydrological response of alpine wetlands to climate warming in the eastern Tibetan Plateau. *Remote Sensing*, 8(4), 336.
- Zhang, X., & Lu, X. (2010). Multiple criteria evaluation of ecosystem services for the Ruoergai Plateau Marshes in southwest China. *Ecological Economics*, 69(7), 1463–1470.
- Zhang, Y., Wang, G., & Wang, Y. (2011). Changes in alpine wetland ecosystems of the Qinghai-Tibetan plateau from 1967-2004. *Environmental Monitoring and Assessment*, 180, 189–199.
- Zhao, J., Jing, Q., Chen, F., & Kun, W. (2009). RS based evaporation estimation of three river sources in Qinghai-Tibet Plateau and its response to lakes and wetlands. *Journal of Jilin University (Earth Science Edition)*, 39(3), 207–513. (in Chinese with English abstract).
- Zhao, Y., Tang, Y., Yu, Z., Li, H., Yang, B., Zhao, W., ... Li, Q. (2014). Holocene peatland initiation, lateral expansion, and carbon dynamics in the Zoige Basin of the eastern Tibetan Plateau. *The Holocene*, 24(9), 1137–1145.
- Zhao, Y., Yu, Z., & Zhao, W. (2011). Holocene vegetation and climate histories in the eastern Tibetan Plateau: Controls by insolation-driven temperature or monsoon-derived precipitation changes? *Quaternary Science Reviews*, 30(9–10), 1173–1184.
- Zhou, L., & Zhou, G. (2009). Measurement and modelling of evapotranspiration over a reed (*Phragmites australis*) marsh in Northeast China. *Journal of Hydrology*, 372(1–4), 41–47.